ORIGINAL PAPER

The variability of South Korean temperature associated with climate indicators

Jai Hong Lee[1] · Pierre Y. Julien[2] · Eric D. Maloney[3]

Abstract

Examining the physical mechanisms through which large-scale climate indicators, e.g., El Niño–Southern Oscillation and Indian Ocean Dipole, affect hydroclimatic variables in the tropics and extratropics is a forefront scientific challenge. We examined climatic teleconnections between large-scale climate indices and temperature variability over South Korea. To do this, we calculated not only leading patterns of observed monthly mean and extreme temperature through an empirical orthogonal teleconnection (EOT) decomposition technique but also statistical correlations on a monthly basis using cross-correlation and lag regression analyses for the leading modes and global atmospheric circulation dataset. As a result, the spatial pattern of the leading EOT modes for mean (extreme high) temperature represents an eastern (southern) coastal mode for boreal summer and a northern (middle) inland mode in boreal winter, while extreme low EOTs exhibit a northern inland mode in summer and a western coastal mode in winter. The temporal evolution of the leading EOT modes exhibits a mostly increasing trend and an interdecadal oscillation. The leading EOT modes of mean temperature explain more variance than those of extreme temperature during warm and cold seasons. The findings from this study illustrate that tropical ENSO forcing has a coherent association with August and December temperature patterns, while the Indian Ocean Dipole is identified as a driver for temperature variability during fall season. The monsoon circulation over the western North Pacific also exhibits a significant negative correlation with the December temperature EOTs. The leading EOTs for October temperature exhibit the positive correlation with the tropical cyclone variability, while the leading EOTs for mean and extreme high temperature exhibit significant negative correlations with the snow depth over northeastern Eurasia in November. The leading patterns of the August and December mean temperature time series are predictable at up to 5-month lead time from the tropical Pacific sea surface temperatures (SSTs), while a predictable response from Indian Ocean SSTs was detected at up to 4-month lead time.

1 Introduction

South Korea experiences spatiotemporal variability of temperature. Temperature varies with fluctuations of various global-regional-scale climate indices (CIs), such as the El Niño–Southern Oscillation, Indian Ocean Dipole, and western North Pacific monsoon activity. These large-scale climate indicators have been widely studied because the extreme phases of these indicators can produce major extremes such as unusually severe cold weather and abnormal heat waves in many regions of the globe. In global- and regional-scale studies, significant relationships have been reported between the large-scale CIs and hydrometeorological variables such as temperature, precipitation, and streamflow in the tropics and extratropics.

The effects of the El Niño–Southern Oscillation (ENSO) on temperature variability on a global and regional scale have been previously documented. Since the first investigation of Walker (1923) on the influence of the Southern Oscillation (SO) on rainfall fluctuations in the Indian monsoon, many recent global-scale studies have documented climatic links between ENSO tropical ocean sea surface temperature variability and global temperature and precipitation anomaly patterns (e.g., Bradley et al. 1987; Kiladis and Diaz 1989; Halpert and Ropelewski 1992). In addition, regional-scale studies in low and middle latitudes (e.g., van Loon and Madden 1981; Ropelewski and Halpert 1986; Redmond and Koch 1991;

✉ Jai Hong Lee
    jlee26@scsu.edu

[1] Department of Civil and Mechanical Engineering, South Carolina State University, Orangeburg, SC 29115, USA

[2] Department of Civil and Environmental Engineering, Colorado State University, Fort Collins, CO 80523, USA

[3] Department of Atmospheric Science, Colorado State University, Fort Collins, CO 80523, USA

Kiladis and van Loon 1988) have revealed statistically significant correlations between regional temperature and ENSO forcing. For example, Ropelewski and Halpert (1986) and Kiladis and Diaz (1989) revealed that North American temperature has a tendency for significant winter temperature anomalies during the ENSO years.

Meanwhile, the Indian Ocean Dipole (IOD) has been considered as one of the key CIs of climate variability for the Indian and Pacific Rim countries. Some studies of the IOD have noted the distinct behavior of the IOD-related temperature anomalies relative to ENSO and other phenomena. Saji and Yamagata (2003) described the significant impact of IOD thermal forcing on large-scale climate anomalies through regression and correlation analyses and revealed that the western tropical Indian Ocean regions show a clear pattern of warm temperature anomalies, while the eastern regions of equatorial Indian Ocean exhibit cool anomalies. The IOD influence on temperature also extends to other regions. For example, Ziao et al. (2002) conducted a diagnostic study using correlation analysis between an IOD index and the temperature data of 160 observation stations in China and showed a significant correlation of Indian Ocean SST with winter temperature in South China.

Several recent studies for the Korean peninsula have also suggested statistically significant responses of temperature variability to large-scale CIs. In an investigation of Korean climate variations for ENSO years, Cha et al. (1999) examined climate variations on the Korean peninsula during extreme phases of ENSO using synoptic data and ECMWF (ERA-15) grid data, and showed that the temperature over Korea in El Nino (La Nina) year is lower (higher) than normal in summer and higher (lower) than normal in winter. Lee and Julien (2015) revealed that cold and warm ENSO phases are the dominant drivers of temperature fluctuations over South Korea based on harmonic and lag correlation analysis. Ha (1995) applied correlation analysis to interannual variability of Seoul wintertime air temperature patterns and documented a prominent teleconnection with tropical sea surface temperatures (SSTs). Ahn et al. (1997) investigated the climatic link between the winter and summer air temperature over five metropolises in South Korea and fluctuations of western-central Pacific SST, and provided evidence of teleconnections between SST anomalies in a particular region of the equatorial Pacific Ocean and regional climate variables. Kang (1998) investigated the correlation of ENSO with Korean climate variability using multichannel singular spectrum analysis and demonstrated significant influences of El Niño and La Niña on winter climate in Korea. In a diagnostic investigation using harmonic analysis on the teleconnection between South Korean temperature and extreme phases of the SO, Lee (1998) revealed that the temperature patterns are significantly correlated with SST anomalies on a monthly basis. Cha (2007) investigated the relationship between ENSO and IOD mode events

and climate variations on the Korean peninsula, and indicated that monthly mean temperature in 11 stations in Korea was higher in winter during El Niño years.

As described above, almost all aforementioned regional and global approaches concentrate on seasonally based temperature variations, and relatively little attention has been given to the far-reaching effects of climate indicators on monthly mean and extreme temperature variability. Also, these studies have focused mostly on the global-scale remote influences of large-scale modes of climate variability through perturbations to the large-scale ocean-atmospheric circulations, and less on the influence of both global and regional CIs on regional- and local-scale temperature. Hence, there has been less focus in the literature concerning the climate impacts of both global and regional CIs on temperature variability. However, the influence of CIs on the East Asian climatology is not limited to the global-scale remote CIs, highlighting a gap in knowledge that requires the need for more information about the overall features of the thermodynamic impacts modulated by various CIs. Thus, it is necessary to investigate systematically how both global and regional CIs affect mean and extreme temperature variability in East Asian regions. In a global-scale study, Halpert and Ropelewski (1992) revealed a consistent climatic link between ENSO forcing and temperature patterns in regions across the world, with indication of a negative signal over the East Asia. From visual inspection of the station location map in their paper, a significant CI-temperature relationship over East Asia cannot be completely discerned because of station coverage limitations. In the present study, we are motivated to expand on previous work by diagnosing the influences of global and regional CIs on temperature variability over South Korea using an expanded surface dataset that can resolve local and regional features.

The present study aims to (1) investigate the spatial pattern and temporal behavior of mean and extreme temperature anomalies over South Korea through an empirical orthogonal teleconnection (EOT) decomposition method, (2) identify significant teleconnections between these leading EOT modes of Korean temperature variability and climate indicators that represent large-scale climate fluctuations and regional synoptic circulations, and (3) demonstrate the predictability of mean and extreme temperature patterns through knowledge of sea surface temperature (SST) anomalies, using regression of the EOT modes onto the SST fields at varying lead times.

## 2 Temperature data and climate indices

The monthly temperature gridded dataset was derived from station-based observed temperature data covering the entire Korean peninsula. The observational data were obtained from the Korea Meteorological Administration (KMA), an affiliated organization of the Ministry of Environment (MOE). The

total temperature time series cover more than 20 ENSO events spanning the time period 1904 through 2015. The observational records are selected only if they have less than a month of missing data, and each monthly temperature data record is required to cover at least 43 years of observation between the years 1973 and 2015, thus spanning at least ten ENSO episodes. Using these criteria, 60 stations were used in our analysis as shown in Fig. 1. In order to estimate high-resolution temperature data with a regular-spaced grid, Parameter-elevation Regression on Independent Slope Model (PRISM) developed by Daly et al. (1994) was employed for the observational temperature data. This model is an independent model for each target grid which can estimate target grid value by weighting each station differently based on the similarity in elevation, distance, topographic facet, and coastal proximity between observational station and target grid. Using this

method, we produced grid data (0.25° × 0.25°) of mean and extreme temperature on a monthly basis from 1973 to 2015.

For comparative analysis between large-scale climate indicators and temperature EOT patterns, several CIs were applied in this present study. Taking into account both atmospheric and oceanic fluctuations, we employed the Multivariate ENSO Index (MEI) as an indicator for tropical ENSO forcing. The MEI is derived from the leading modes calculated by an EOF decomposition technique for several air-sea variables over the tropical Pacific Ocean, including SST, SLP, surface air temperature, cloudiness fraction, and zonal-meridional surface wind (NOAA-Earth System Research Laboratory, Physical Sciences Division). Because it integrated both atmospheric and oceanic factors related to ENSO, the MEI may be considered as a better indicator of ENSO relative to other single-variable CIs (Karabörk and Kahya 2007). In this

Fig. 1 Gridded temperature data with stations
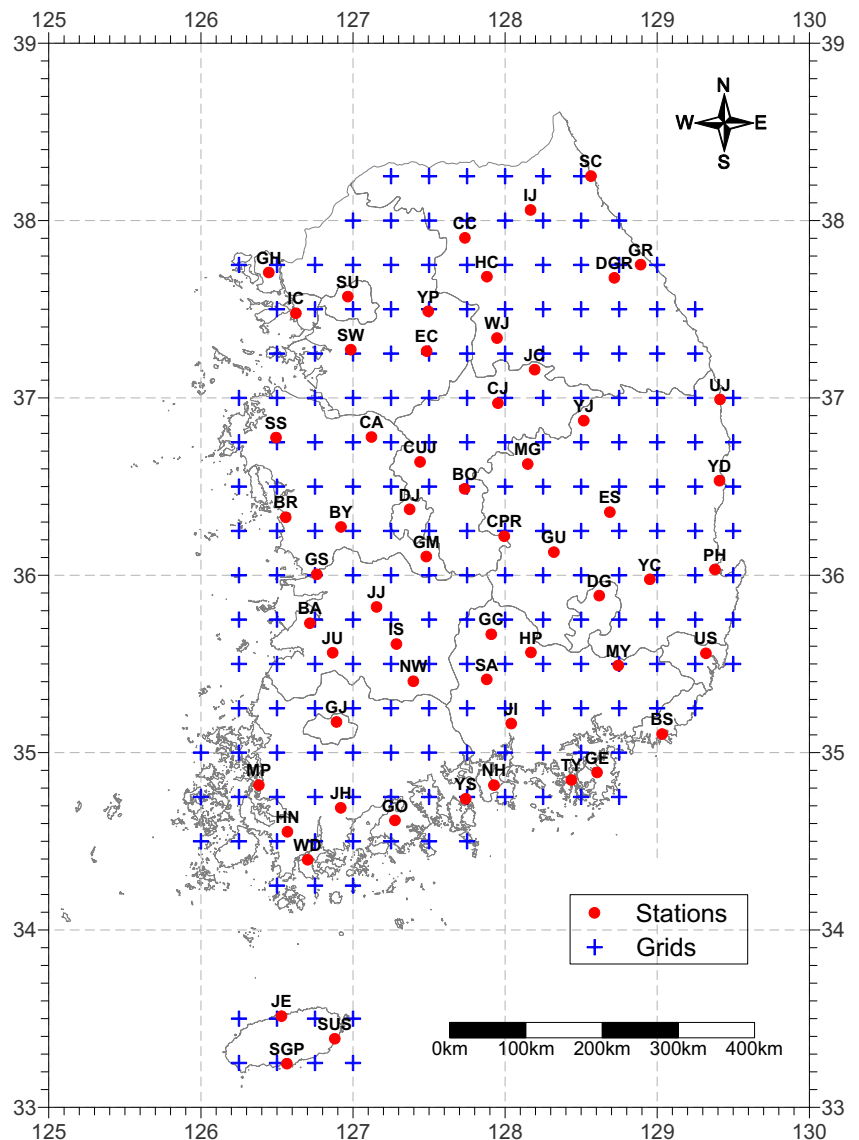
analysis, we employed the standardized bimonthly MEI values regularly updated by the Climate Diagnostic Center (CDC) that start in December 1949–January 1950. As an indicator of the IOD, we employ the Dipole Mode Index (DMI) similar to the empirical approach by Saji et al. (1999). This index that we obtain from the NOAA Climate Prediction Center represents the magnitude of the anomalous SST gradient from the southeastern (90° E–110° E, 10° S–0°) to the western (50° E–70° E, 10° S–10° N) near-equatorial Indian Ocean and is derived from the Hadley Centre Global Sea Ice and SST (HadISST) dataset. In the current analysis, the DMI index was employed in cross-correlation analysis as well as partial correlation analysis with the EOT time series to remove the linear influence of the ENSO forcing on temperature variability.

To confirm the relationship between the large-scale climate variation and the EOT modes for mean and extreme temperature, we employ SST and atmospheric circulation datasets. For SST data, the Extended Reconstructed SST (ERSST.v4) datasets (Huang et al. 2014) are used in this study due to the fact that the SST in ERSST.v4 exhibits a substantially more realistic El Niño/La Niña behavior in the period of the record when data are sparse and therefore a better estimate of long-term variability in climate dataset (Huang et al. 2014). The ERSST is a global monthly SST dataset calculated based on the International Comprehensive Ocean and Atmosphere Dataset (ICOADS), which is widely used in global- and regional-scale studies. It is provided on a 2.0° × 2.0° grid that uses statistical techniques to provide global coverage and spans the period from January 1854 to the present. The global atmospheric circulation fields are obtained from the reanalysis derived from the joint project of the National Centers for Environmental Prediction-National center for Atmospheric Research (NCEP-NCAR), which are available on NOAA-Earth System Research Laboratory, Physical Sciences Division. This dataset is continually updating to produce fields on a 2.5° × 2.5° grid using a state-of-the-art numerical modeling system for prediction and data assimilation with continuously entrained observations. The monthly NCEP-NCAR reanalysis dataset is available for the period from 1948 to present.

Links between temperature EOTs and monsoon circulation variability are investigated using the WNPMI index over western North Pacific. Using the methodological approach in Wang et al. (2013), the WNPMI index is calculated based on the difference between 850-hPa zonal winds (U850) in the region 5–15° N, 100–130° E and the region 20–30° N, 110–140° E. The former region represents the intensity of the monsoon westerlies from Indochina Peninsula to the Philippines, while the latter indicates the magnitude of the easterlies over the southeastern part of the WNP subtropical anticyclone. The monthly Tropical Cyclone Index (TCI) quantifying the tropical cyclone activity is calculated based on the tropical cyclone tracks recorded by the IBTrACS (Knapp et al. 2010) and the National Typhoon Center (NTC) of KMA. For the period from 1973 through 2015, the TCI is obtained from the frequency of tropical cyclones passing through the index area as shown in Fig. 2. The monthly Eastern Eurasian Snow Index (EESI) is employed to examine the impact of the snow depth over northeastern Eurasia on the temperature pattern of the Korean peninsula. The EESI is derived from area-mean time series of snow depth over Eastern Eurasian north of the Korea-Japan (EENKJ; 46°–60° N, 120°–140° E) as estimated by Kripalani et al. (2010).

3 EOT and statistical analyses

The general methodology used in this present analysis, which follows the comprehensive empirical approach by Van den Dool et al. (2000), can be briefly summarized as follows and is described in more detail below. The first step is to convert the original data to a monthly time series for mean and extreme temperatures. Then, empirical orthogonal teleconnection (EOT) techniques are performed for identification of the spatiotemporal variability of mean and extreme temperatures over South Korea. The next step is to conduct both cross-correlation analysis and linear regression analysis to quantify the teleconnection between global and regional CIs and principal temperature modes. The final step is to perform a lag regression analysis using the regression of SST data onto EOT modes with varying lead times to examine the potential predictability of mean and extreme Korean temperatures relative to Pacific tropical thermal forcing.

In this present analysis, extreme temperature time series are generated following the recommendation of the Climatic Variability and Predictability (CCI/CLIVAR) panel. The monthly highest/lowest five consecutive day average temperature is employed to define extreme high/low temperatures. During the period from 1973 to 2015, the monthly mean and extreme temperature time series are calculated for each station. As mentioned above, only KMA gauging stations in which the time series of the mean and extreme temperature have less than a month of missing data and the monthly temperature data cover at least 43 years of observations are used in this study.

Prior to the EOT analysis to examine the CI-temperature teleconnection, we converted the temperature data to a Standardized Temperature Index (STI) formulated for effective assessment of wet and dry condition as described by McKee et al. (1993) and Lee and Julien (2016, 2017). The STI is calculated as follows. First, the monthly temperature data are transformed into a time series fitted to a particular probability distribution function for each month. Then, the fitted frequency distribution function is converted to a cumulative distribution function (CDF) using a standard normal
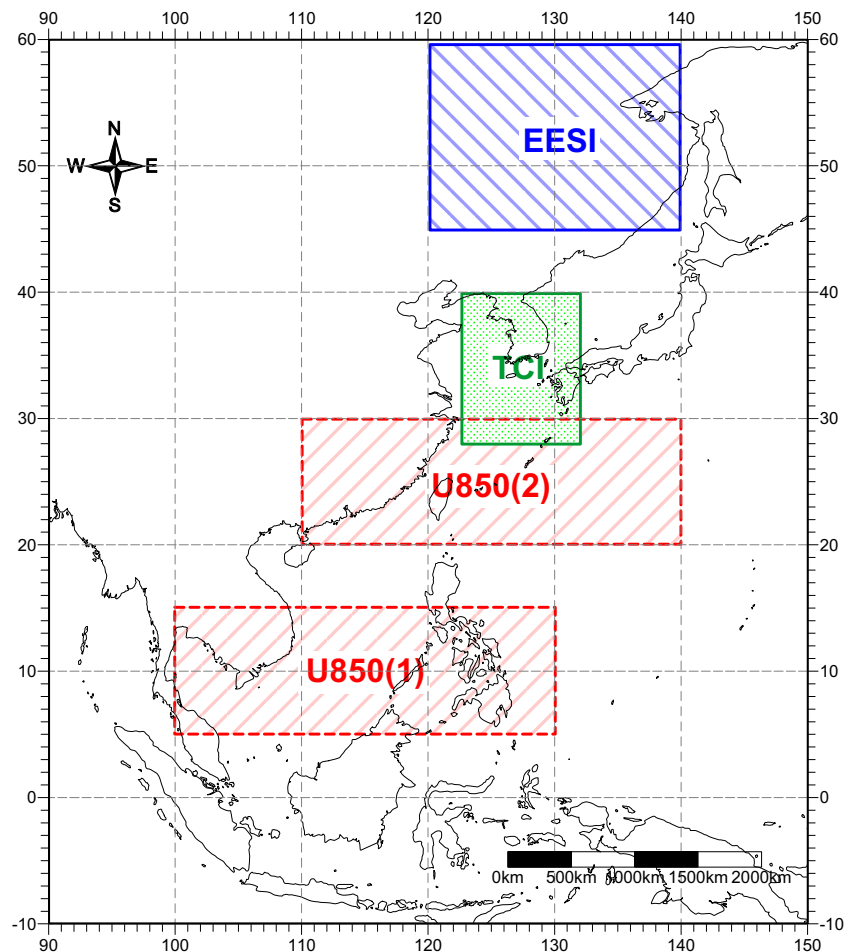
distribution based on an equal-probability condition. Finally, the STI dataset which is used in the EOT process is processed to have zero mean and unit variance using the above CDF. The STI is very straightforward to estimate because one variable is used as input data, and is easy to compare from a spatial and temporal viewpoint since the index is presented as dimensionless.

For the purpose of investigating spatiotemporal patterns of mean and extreme temperature over South Korea, we employ the empirical orthogonal teleconnection (EOT) decomposition technique reported by Van den Dool et al. (2000), rather than a classical empirical orthogonal function (EOF) analysis. Due to the fact that EOT decomposition technique is orthogonal in one either space or time, while EOF is orthogonal in both space and time, EOT method provides a potentially more intuitive interpretation of the resulting patterns. King et al. (2014) examined Australian monthly precipitation variability through EOT decomposition analysis and found that the first December EOT mode shows notable predictability up to several month (1 year) in advance given knowledge of tropical Pacific Ocean (Indian Ocean) SST. Also, in a diagnostic study to understand the physical mechanisms behind the effects of large-scale climate indices on precipitation patterns in

Queensland, Australia, Klingaman et al. (2013) used EOT decomposition to identify remote and local drivers affecting the interannual and decadal variability of seasonal precipitation patterns. Stephan et al. (2018a, b) employed the EOT analysis in order to identify regions in China showing coherent interannual/intraseasonal variabilities in precipitation and to understand the precipitation-related local- and large-scale atmospheric and coupled atmosphere–ocean processes.

EOT analysis decomposes a temperature dataset with spatiotemporal variability into a set of orthogonal components, namely EOT patterns. The first EOT spatial modes are obtained by finding the point that explains the most of the variance at all other points, which is designated as a base point by Van Den Dool et al. (2000). Then, the temperature time series of the base point is defined as the first temporal mode of the temperature pattern. The second EOT spatial modes are extracted by removing the influence of the base point on all other points using regression analysis for temperature time series of the base point and all other points. From this modified temperature dataset, the second base point is identified by detecting the point explaining the most variance of the residual temperature record. This procedure is repeated for subsequent modes until the desired number of modes is derived. Following

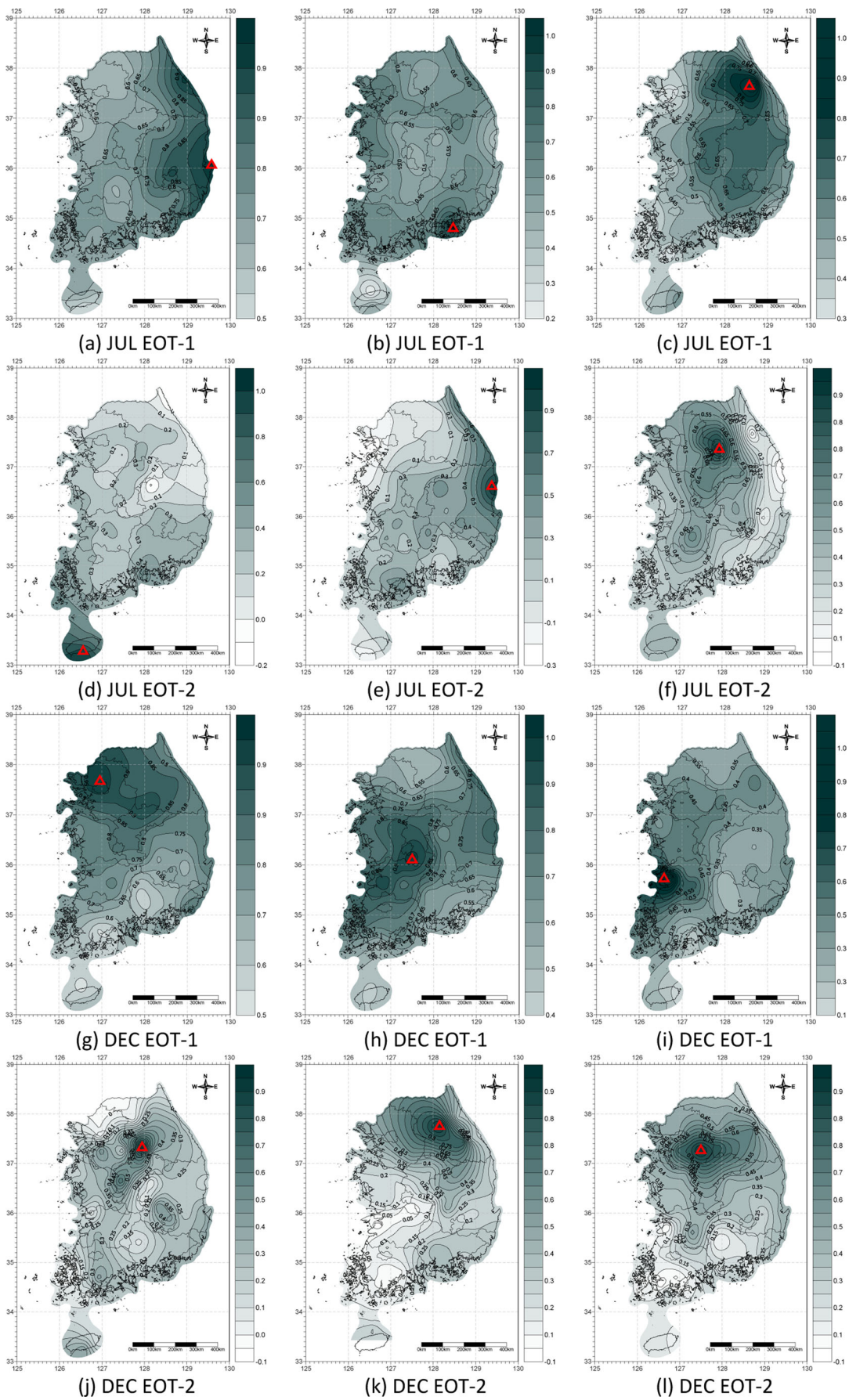Fig. 2 Map of climate indices boundary

(a) JUL EOT-1

(b) JUL EOT-1

(c) JUL EOT-1

(d) JUL EOT-2

(e) JUL EOT-2

(f) JUL EOT-2

(g) DEC EOT-1

(h) DEC EOT-1

(i) DEC EOT-1

(j) DEC EOT-2

(k) DEC EOT-2

(l) DEC EOT-2

Fig. 3 Maps of the locations of each EOT and the correlations between EOT time series (i.e., base point time series) and time series at all other grid points for the first and second EOTs of July and December mean (left), extreme high (middle), and extreme low (right) temperatures. Triangles indicate the base points

the procedure above, EOT-1 and EOT-2 were obtained for monthly mean and extreme temperature time series during 1973–2015 to investigate patterns of temperature fluctuations across South Korea.

Following the approach by King et al. (2014), correlation coefficients between the temperature EOT modes and various CIs are calculated using Spearman's correlation analysis with statistical significance assessed at the 5% level taking into account the fact that some CI time series may not exhibit a normal distribution. Although the correlation analysis was performed by Spearman's rank test, the resultant correlation coefficients were in general agreement with those calculated by the commonly used Pearson's correlation method (not shown here). The overall findings from correlation and regression analyses between temperature EOT modes and various CIs are described using correlation and regression maps.

4 Spatial and temporal structures of EOTs

The EOT modes for mean and extreme temperatures were extracted from the mean and extreme temperature time series for the period of 1973–2015. Correlation maps for each EOT associated with the highest value of explained variance were plotted for each month. The values displayed in these maps are the correlation coefficients between the temperature EOT

time series at the base point and the temperature time series at all other points. Each leading EOT has the most explained variance for mean and extreme temperatures. The spatial patterns of the leading EOT base points and highest correlation values for each month reflect the climatological seasonal pattern of temperature combined with the influence of midlatitude weather systems on the Korean peninsula. The second EOT is also computed using the procedures discussed above. Figure 3 shows the resultant patterns for the leading two EOTs of July and December mean (Tm), extreme high (Tx5), and extreme low (Tn5) temperatures (hereinafter referred to as Tm, Tx5, and Tn5).

The base points of the first EOTs for mean and extreme temperatures show different locations with respect to season. The locations of base points for mean temperature are different from those for extreme temperatures during the summer months. The base point for Tm-EOT is located in the east coastal area of South Korea, whereas those for Tx5-EOT and Tn5-EOT are located in the southern and northern inland. In the winter months, the base points of leading Tm-EOTs have a tendency to shift northward, but less so for the extreme temperature time series that shifts to central South Korea. In addition, for entire months as shown in Table 1, we categorized total EOTs into coastal (west/south/east) and inland (north/middle/south) modes that take into account the locations of the base points. The centers of the total leading EOT modes are categorized into coastal area (28 modes) and inland area (44 modes). Overall, the lower-order EOT modes show more variability in the locations of the base points.

Locations of the base points indicate that out of 24 Tm/Tx5/Tn5 EOTs consisting of the leading two EOTs for each

Table 1 Explained variance (VE) for the two leading EOTs of monthly mean and extreme temperatures with the center of the leading mode, which is listed in parentheses: EC (east-coast mode), SC (south-coast mode), WC (west-coast mode), NL (north-inland mode), ML (middle-inland mode), and SL (south-inland mode). Underlined indicates the nationwide spatial patterns. Triangles, inverted triangles, and circles indicate increasing, decreasing, and interdecadal temporal patterns respectively

Mode	Jan	Feb	Mar	Apr	May	Jun	Jul	Aug	Sep	Oct	Nov	Dec
Mean temperature (Tm)												
EOT-1	0.64	0.69	0.63	0.59	0.46	0.51	0.61	0.64	0.53	0.58	0.69	0.68
	(NL) ●	(NL) ●	(ML) ▲	(NL) ●	(ML) ▲	(NL) ▲	(EC) ●	(EC) ●	(ML) ▲	(NL) ▲	(NL) ▲	(NL)
EOT-2	0.18	0.14	0.15	0.16	0.22	0.21	0.25	0.17	0.18	0.16	0.15	0.14
	(SC) ●	(EC) ●	(EC) ●	(EC) ▲	(EC) ●	(EC) ●	(SC) ●	(SC) ▲	(SL) ▼	(ML) ▼	(ML) ▼	(NL) ▲
Extreme high temperature (Tx5)												
EOT-1	0.64	0.68	0.51	0.39	0.41	0.36	0.51	0.48	0.53	0.43	0.68	0.68
	(SL) ●	(EC) ●	(NL) ●	(WC) ●	(SL) ●	(EC)	(SC)	(SL)	(SL) ▲	(NL)	(ML) ▲	(ML)
EOT-2	0.21	0.18	0.19	0.28	0.20	0.22	0.18	0.26	0.16	0.21	0.18	0.19
	(NL)	(SL) ●	(EC) ●	(EC) ▲	(WC)	(NL)	(EC) ●	(NL) ▲	(EC)	(EC)	(NL)	(NL) ●
Extreme low temperature (Tn5)												
EOT-1	0.58	0.65	0.50	0.48	0.47	0.48	0.60	0.52	0.52	0.54	0.52	0.48
	(NL) ●	(NL) ▲	(SC)	(ML) ▲	(SL) ●	(NL)	(NL)	(NL)	(NL) ▲	(SC) ▲	(NL) ▲	(WC)
EOT-2	0.21	0.19	0.17	0.15	0.25	0.25	0.22	0.24	0.23	0.18	0.17	0.29
	(SL) ●	(WC)	(NL)	(NL)	(EC) ▲	(SC) ▲	(NL) ▲	(ML)	(SC) ●	(SC) ▼	(SL)	(NL)

of 12 months, 10/10/8 are identified as coastal modes and 14/14/16 are identified as inland modes as shown in Table 1. Breaking this into more detail, the coastal mode consists of an east-coast mode 7/7/1, south-coast mode 3/1/5, and west-coast mode 0/2/2 defined on the basis of the center of leading mode. Also, the inland mode consists of the north-inland mode 8/7/11, middle-inland mode 5/2/2, and south-inland mode 1/5/3. Consistent with the patterns shown in Fig. 3, Table 1 indicates that the leading Tm-EOT (Tx5-EOT) modes represent an eastern (southeast) coastal mode for boreal summer season and a northern (middle) inland mode in winter season, while the leading Tn5-EOT mode exhibits a northern inland mode in summer and a western coastal mode in winter.

The total spatiotemporal variance related to the two leading EOTs varies as a function of months. Table 1 shows that the spatiotemporal variance related to Tm/Tx5/Tn5 EOT modes ranges from 0.46 to 0.69/0.39 to 0.68/0.47 to 0.65 for each first EOT mode, while that for EOT-2 decreases on average to 0.17/0.20/0.21 at each month. Explained variance for the leading Tm-EOTs is higher than that associated with the first Tx5- and Tn5-EOTs in all months due to the fact that mean variables are more likely to be characterized by spatially homogeneous features as opposed to extreme variables having more spatial incoherence (King et al. 2014).

Temporal behavior is now diagnosed for each of the EOT modes of mean and extreme temperatures using moving average line employed by Kim et al. (2004) who defined temporal evolution of decomposed precipitation time series as increasing, decreasing, and interdecadal patterns based on 5-year running mean plots. Figure 4 indicates time series for the leading two modes for 2 months (January and September), and Table 1 summarizes characteristics for all the months. For the Tm-EOT modes, 9 exhibit an increasing trend, 3 a decreasing trend, and 11 an interdecadal variability (Table 1). The Tx5/Tn5 EOT time series show 13/13 significant trends, including 4/8 having increasing trends and 9/4 with interdecadal fluctuations. The temporal evolution of the leading EOT modes indicates increasing trends during fall season and primarily an interdecadal oscillation for winter season. Jung et al. (2002) investigated temperature changes over South Korea since 1954, both in terms of means and extreme events, using observational station data, and indicated
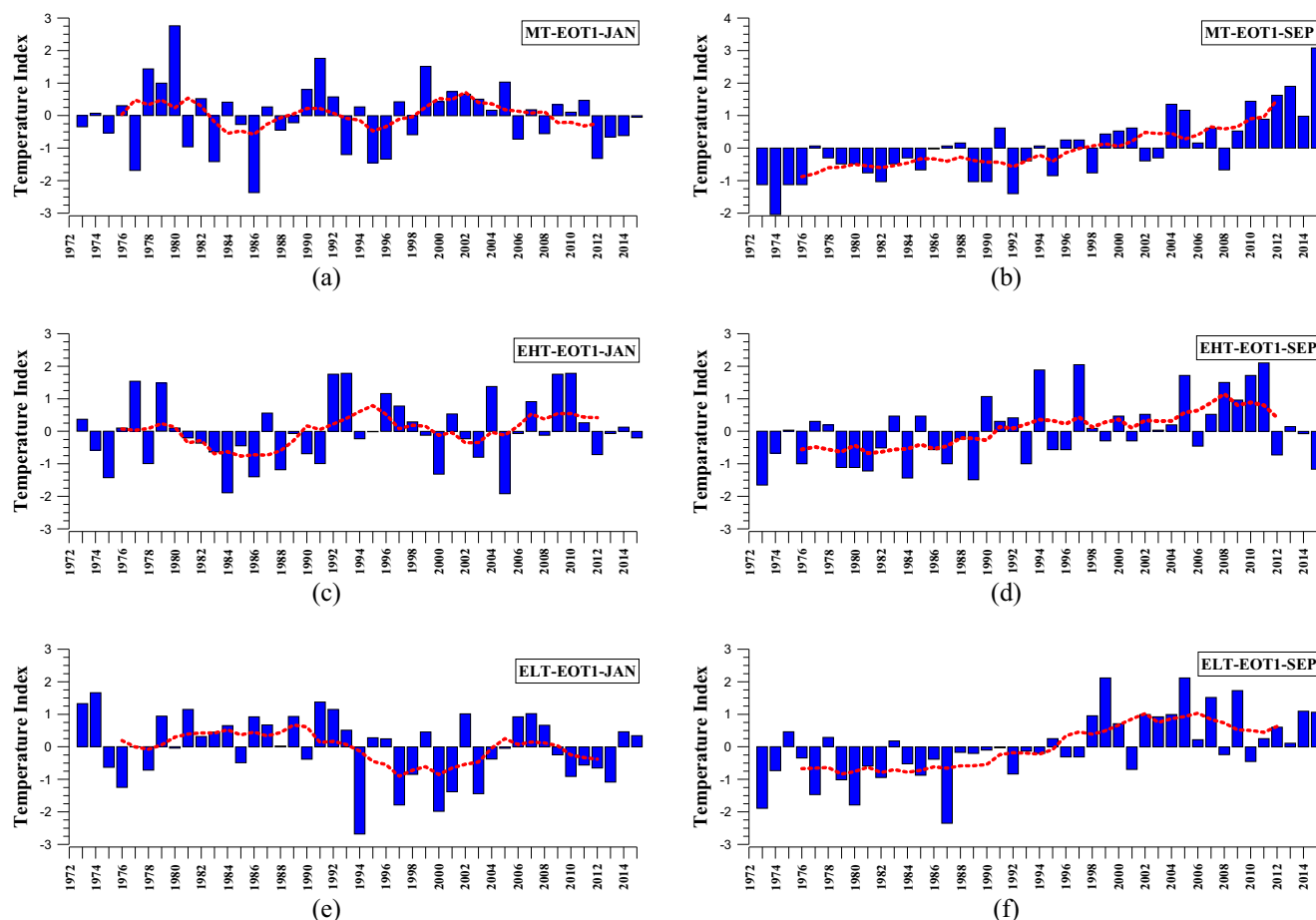

Fig. 4 Annual time series (bars) and their 7-year running means (thick lines) for the EOT-1 with increasing trend and interdecadal cycle. The upper panels are the temporal cycles for mean temperature, the middle panels are those of extreme high temperature, and the lower panels are those of extreme low temperature

that climatic extremes have increased during recent decades. The frequent occurrence of extreme maximum temperature events shows an increasing trend, with higher values in recent decades. Thus, it is plausible that the frequency of extreme temperature events plays an important role in the long-term temporal increasing trends of temperature.

5 Teleconnections between EOTs and CIs

For the purpose of investigating the teleconnected effects of various climate indices on mean and extreme temperature variability across South Korea, the temperature EOT modes were correlated with several climate indices representing spatially and temporally significant variability. We mainly discuss outcomes involving mean temperature EOTs, except where extreme temperature EOTs show noticeably different results compared to those of mean temperature EOTs. The correlation coefficients of each EOT with various CIs are shown for mean and extreme temperature in Table 2. In addition, regression maps for NCEP-NCAR reanalysis MSLP and ERSST.v4 SST are shown in Fig. 5 for EOT-1 during December, and maps for other modes are also discussed. Many regression maps indicate notable signals consistent with the large-scale spatial patterns reported in other studies.

The correlation coefficients for EOT-1 and EOT-2 versus the MEI are shown in Table 2. The MEI time series has significant negative correlations with the leading EOTs for mean temperature in August and September, whereas the leading EOT for December exhibits a positive correlation with the

ENSO forcing. In spring and summer months, the SST-related signal associated with ENSO is weaker and not significant (not shown here). In addition to the leading EOTs, the other lower-order EOTs show relatively significant correlations in some months with ENSO indices in eastern and southern coastal areas of South Korea (not shown here). The findings from the above correlation analysis suggest that the El Niño (La Niña) events make conditions more favorable for above (below) normal mean temperatures in eastern coastal and northern inland areas of South Korea. The extreme temperature EOTs also have significant correlations with ENSO indicators. The MEI shows higher correlation coefficients with the extreme temperature EOTs in October and December than other times of the year.

The linkages between the temperature EOT modes and the ENSO indicators can also be identified through regression analysis, as shown in Fig. 5. Positive EOT temperature modes exhibit an SST anomaly pattern consistent with a typical ENSO SST warm event, consisting of warmer SST anomalies over the central-eastern tropical Pacific and cooler SST anomalies in the western equatorial Pacific Ocean (Fig. 5a, c, e). Above-normal signals in many mean and extreme temperature EOTs are closely related to ENSO-like SST patterns. In addition to the tropical Pacific SST pattern, regressing MSLP onto the first EOT modes for mean and extreme temperature (Fig. 5b, d, e) describes similar ENSO-like SLP patterns with higher pressure in the western North Pacific and lower pressure in the eastern North Pacific region. This pattern reflects the Pacific-East Asian teleconnection (PEA) pattern which represents a damping of the East Asian winter monsoon

Table 2 Correlation coefficients of the two leading EOTs of monthly mean and extreme temperature with climate indicators: MEI (Multivariate ENSO Index), IOD (Indian Ocean Dipole), WNPMI (Western North Pacific Monsoon Index), TCI (Tropical Cyclone Index), and EESI (Eastern Eurasia Snow Index). The bold, single underlined bold, and double underlined bold indicate correlations that are statistically significant at the 0.10, 0.05, and 0.01 levels

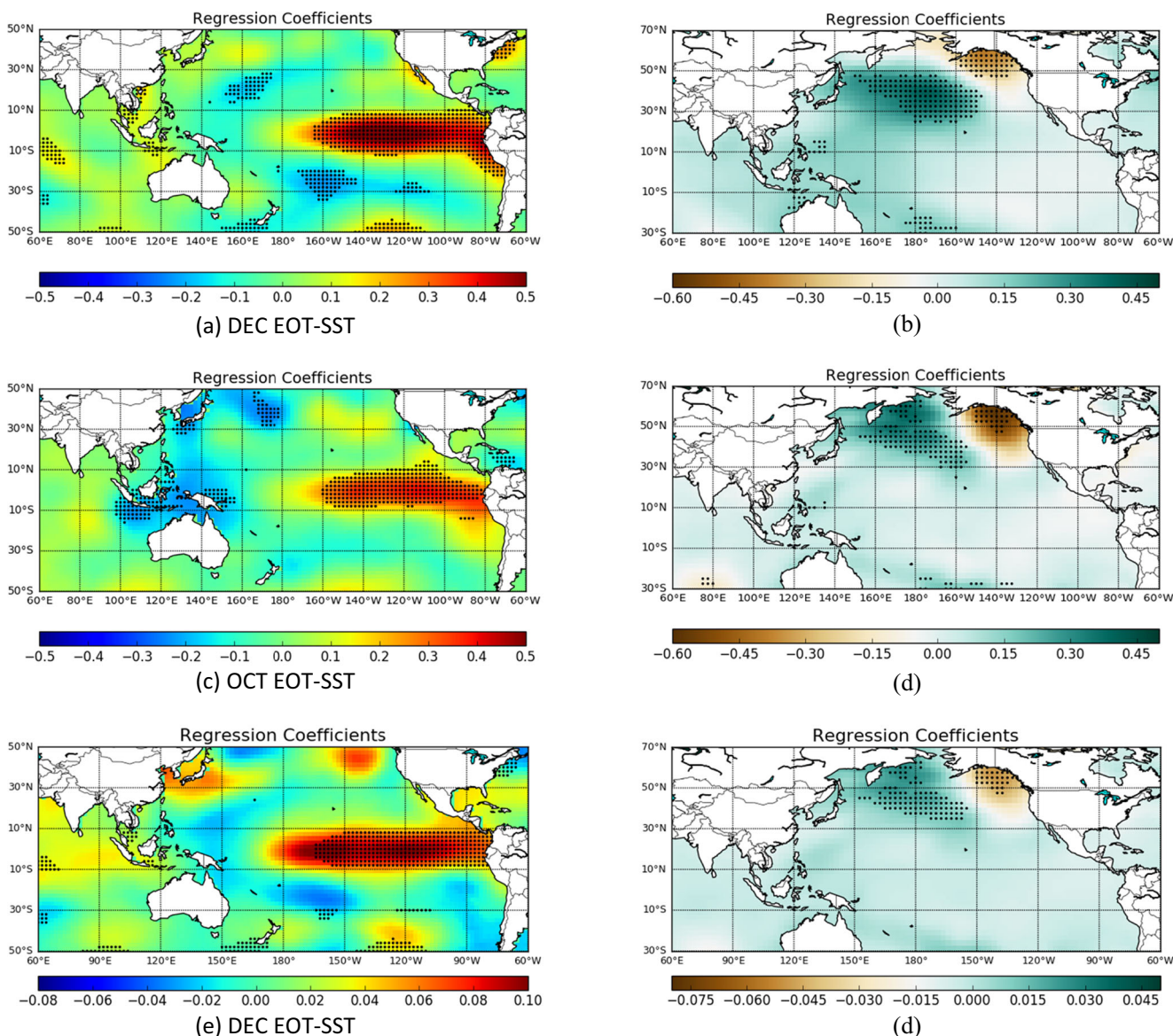| Mode	Mean temperature (Tm)					Extreme high temperature (Tx5)					Extreme low temperature (Tn5)				
	MEI	IOD	WNP	TCI	EESI	MEI	IOD	WNP	TCI	EESI	MEI	IOD	WNP	TCI	EESI
EOT-1															
Aug	−**0.42**	0.11	**0.29**	0.09	0.14	−0.08	0.09	**0.27**	0.11	0.08	−**0.26**	0.17	0.18	0.08	0.04
Sep	−**0.30**	0.13	0.13	0.12	0.09	−0.07	**0.31**	0.20	0.14	0.11	−0.09	**0.33**	0.17	0.11	0.10
Oct	0.03	**0.33**	0.02	**0.31**	0.24	**0.31**	**0.39**	0.03	**0.28**	0.01	−0.11	0.02	0.19	0.14	0.09
Nov	**0.26**	**0.36**	−0.05	−0.03	−**0.33**	0.18	0.13	−0.01	−0.02	−**0.28**	0.12	**0.31**	−**0.26**	−0.12	−0.13
Dec	**0.39**	−0.05	−**0.32**	–	0.12	0.09	−0.11	−**0.29**	–	0.10	**0.34**	0.11	0.01	–	0.17
EOT-2															
Aug	0.11	0.18	0.18	0.05	0.11	−0.12	**0.29**	−0.08	0.11	0.12	−**0.29**	0.02	−0.06	0.13	0.14
Sep	−**0.33**	−**0.30**	0.07	0.09	0.01	−0.05	−0.02	−0.14	0.05	0.17	0.08	−0.19	−0.02	**0.26**	0.02
Oct	−0.09	−**0.27**	0.18	0.18	0.14	0.11	0.17	0.02	0.16	**0.26**	−0.07	−0.17	0.04	0.12	0.24
Nov	0.02	−0.08	**0.28**	−0.29	0.29	0.04	0.18	0.05	**0.28**	0.02	0.01	0.21	0.01	0.16	0.08
Dec	0.21	**0.26**	0.02	–	0.08	0.01	−0.12	0.13	–	0.05	−0.03	−0.14	0.18	–	0.01

Fig. 5 Maps of SST (left) and MSLP (right) regressed on to the leading EOT of mean (upper), extreme high (middle), and extreme low (lower) temperature

induced by a western North pacific anticyclone and ENSO warm phases over the eastern equatorial Pacific Ocean (Wang et al. 2000). This phase of the PEA teleconnection preferentially modulates mean and extreme temperatures over South Korea during ENSO events.

The IOD is also associated with mean and extreme temperature variability in South Korea. As shown in Table 2, the first and second mean temperature EOT modes are significantly correlated with the IOD as quantified by the DMI index representing the anomalous SST gradient between the western and eastern tropical Indian Ocean. Both October and November EOT-1 for mean temperature exhibits a northern inland mode exhibiting a positive correlation with the DMI. The extreme temperature EOT modes also demonstrate a positive significant correlation with the DMI in fall season. The

partial correlation of the DMI index against the EOT modes was also examined to rule out that the IOD was influencing Korean temperature only because of its covariability with ENSO. However, the resultant number of significant relationships was the same as the above result, providing confidence that the IOD influences Korean temperature in a manner independent of ENSO. However, it should be noted that there might be a non-linear dependence as oppose to the linear effect of ENSO on the IOD and Korean temperature.

The correlation coefficient of monsoon circulation activity with each EOT was calculated using the WNPMI index. From the results of correlation analysis in Table 2, the leading EOTs for mean and extreme temperatures exhibit significant negative (positive) correlations with the monsoon variability over the WNP region in December (August). In the negative

WNPMI phase, the atmospheric circulation of the WNP trough is weakened accompanied by a suppression of westerlies over the Philippine Sea. The corresponding weakened atmospheric circulation prevails from Philippine Sea all the way to Japan along the flank of the WNP subtropical high. These circulation anomalies favor warmer than normal temperature along the East Asia including the Korean peninsula (Wang et al. 2000).

The monthly TCI indices were calculated for the index area to the south part of the Korean peninsula (Fig. 2). Each TCI is correlated with the EOT modes for Tm/Tx5/Tn5 from May to November. As shown in Table 2, several EOTs show the significant correlation with the TCI time series, indicating that increased and decreased frequency of tropical cyclones passing through the index area is associated with enhanced and suppressed temperature. The leading EOTs for October temperature exhibit the positive correlation with the tropical cyclone variability. This indicates that the leading EOT in fall season, located in eastern coastal area over the Korea peninsula, shows significant positive correlation with the TCI. The physical link between the tropical cyclone activity and October temperature variability is difficult to construct. Over the western North Pacific, genesis and development of tropical cyclones play a role in Korean climate fluctuation during the fall season. KMA (2018) indicated that the warmer than normal temperature in October is attributed to the frontal warm air mass that the tropical cyclone drives. The frontal air mass by the tropical cyclone brings warm air from the equator to the Korean peninsula leading to warmer than normal temperature activity. The correlation coefficient of snow depth variability with each EOT was calculated using the EESI. From the results of correlation analysis in Table 2, the leading Tm-EOT and Tx5-EOT exhibit significant negative correlations with the EESI in November. This implies that the leading EOT in November, located in northern inland area over the Korean peninsula, shows significant negative correlation with the snow depth over the northeastern Eurasia region. Min and Yang (1998) showed that the temperature gradient by the snow depth is conducive to transport cold and dry air from the north toward south over the East Asia during the fall season.

As shown in Tables 1 and 2, the MEI and WNPMI indices exhibit significant correlation with both inland and coastal modes for mean temperature, while the IOD, TCI, and EESI indices correlate with only the inland modes of Tm-EOT. All climate indices for extreme high temperature (Tx5) show significant correlation with the inland modes. The MEI time series correlate with both inland and coastal modes for Tn5-EOTs, while the IOD and WNPMI indices exhibit significant correlation with only the inland modes for extreme low temperature. The results from this analysis across all climate indices are generally consistent with the previous findings by Cha (2007) that indicate a significant correlation between tropical climate circulations and seasonal temperature patterns over South Korea. Cha (2007) investigated the relationship between ENSO/IOD indices and climate variations on the Korean peninsula using composite analysis with Nino 3.4 SSTs of Japanese Meteorological Agency and IOD data from U.K. Met Office. Although Cha (2007) used different data and methods, the findings are generally consistent with our results in terms of negative response in summer and positive response in winter.

6 Predictability of temperature patterns

In addition to expanding our understanding of how CIs affect Korean temperature variability, it is also of great importance to improve prediction capability of this variability. The previous correlation analysis did not take into account any time lag between the EOT time series for mean and extreme temperatures and various CIs. If the various CIs applied here have a significant impact on the temperature anomaly over South Korea, then it is worthwhile to quantify the degree of this influence by a time-dependent cross-correlation analysis between the two time series that would be useful for forecasting purposes. To do this, we correlated the monthly EOTs for the mean and extreme temperature with CIs at monthly time lags of lag-0 months to lag-17 months, where the EOTs are lagging the CIs. The motivation to focus on the monthly time lag, e.g., a time interval of 0 to 17 months, is based on the fact that the climate signals used here are slowly evolving and this low-frequency behavior may provide substantial value as a long-range predictor. The results of this analysis are presented in Table 3 as the cross-correlation coefficient values. The overall correlation coefficients are calculated at 0.10, 0.05, and 0.01 significance levels for better comparison.

The cross-correlation coefficient between ENSO and each EOT was computed for the MEI. As shown in Table 3, the December EOT-1 exhibits significant positive correlations with the MEI time series up to the preceding July, while the August EOT-1 exhibits the negative correlations with the MEI up to the preceding June. No significant correlation for the ENSO signal was detected during January to July reflecting the fact that relationships between the ENSO indicators and each EOT mode are generally not prominent at this time of year (not shown here). The outcomes from the cross-correlation analysis above indicate that the teleconnected effects of the ENSO phenomena on the leading modes of mean temperature in South Korea are detectable at up to 5-month lead time. Additionally, the leading EOTs for extreme temperature also show significant lagged correlations with ENSO remote forcing as shown in Table 3. The MEI from June to October (August to December) has significant positive correlations with the leading Tx5-EOT (Tn5-EOT) in October (December), but EOT extreme temperature modes derived

Table 3 Cross-correlation coefficients of the leading EOTs of monthly mean and extreme temperature with climate indicators. The bold, single underlined bold, and double underlined bold indicate correlations that are statistically significant at the 0.10, 0.05, and 0.01 levels

Mode	CIs for mean temperature (Tm)							CIs for extreme high temperature (Tx5)							CIs for extreme low temperature (Tn5)						
	Jun	Jul	Aug	Sep	Oct	Nov	Dec	Jun	Jul	Aug	Sep	Oct	Nov	Dec	Jun	Jul	Aug	Sep	Oct	Nov	Dec
Lag EOT for Multivariate ENSO Index (MEI)																					
Aug	**−0.39**	**−0.39**	**−0.40**					−0.06	−0.04	−0.04					−0.20	−0.22	−0.18				
Sep	−0.09	−0.17	−0.19	**−0.28**				0.11	0.09	0.01	−0.02				−0.05	−0.06	−0.07	−0.06			
Oct	0.12	0.08	0.06	0.08	0.07			**0.31**	**0.26**	**0.28**	**0.27**	**0.30**			−0.08	−0.10	−0.08	−0.07	−0.12		
Nov	**0.26**	**0.27**	0.24	0.23	0.20	**0.27**		**0.31**	**0.30**	**0.26**	0.22	0.18	0.14		0.06	0.08	0.11	0.13	0.12	0.14	
Dec	0.19	**0.26**	**0.30**	**0.28**	**0.31**	**0.32**	**0.33**	0.02	0.04	0.08	0.03	0.05	0.05	0.07	0.23	0.24	**0.28**	**0.26**	**0.27**	**0.30**	**0.31**
Lag EOT for Indian Ocean Dipole Index (IOD)																					
Aug	−0.14	0.08	0.11					−0.05	0.06	0.09					−0.28	0.12	0.17				
Sep	0.09	0.14	0.15	0.13				0.15	**0.34**	**0.40**	**0.31**				0.15	0.23	**0.35**	**0.33**			
Oct	**0.33**	**0.29**	**0.40**	**0.32**	**0.33**			**0.27**	**0.26**	**0.30**	**0.31**	**0.39**			0.04	−0.05	−0.01	−0.05	0.02		
Nov	0.15	0.23	**0.30**	**0.39**	**0.40**	**0.36**		0.13	0.08	0.16	0.16	0.17	0.13		0.04	0.19	0.21	**0.30**	**0.26**	**0.31**	
Dec	0.01	0.00	0.05	0.18	0.22	0.04	−0.05	−0.06	0.05	0.06	−0.02	−0.03	−0.18	−0.11	−0.04	−0.01	0.12	**0.26**	**0.28**	0.22	0.11

for other months do not exhibit any significant correlations with the ENSO indices except possibly the November EOT-1 with ENSO signals in June, although this correlation could be spurious. The lagged responses of the leading EOTs for extreme temperature to the MEI indices are different from those for mean temperature. The IOD is also associated with mean and extreme temperature variability in South Korea. In Table 3, the leading EOT for mean temperature in October (November) has positive correlations with the DMI time series up to the preceding June (August). The leading Tx5-EOT

(Tn5-EOT) in September shows positive lagged correlations with the July (August) to September DMI time series, while the IOD index from June to October (September to November) exhibits significant positive correlations with the leading October Tx5-EOT (November Tn5-EOT).

In addition to the cross-correlation analysis, the Pacific Ocean SSTs based on the ERSST.v4 dataset are regressed onto the EOTs at varying lead times to identify potential sources of predictability for monthly mean and extreme Korean temperature. As shown in Figs. 6 and 7, the above lag regressions of
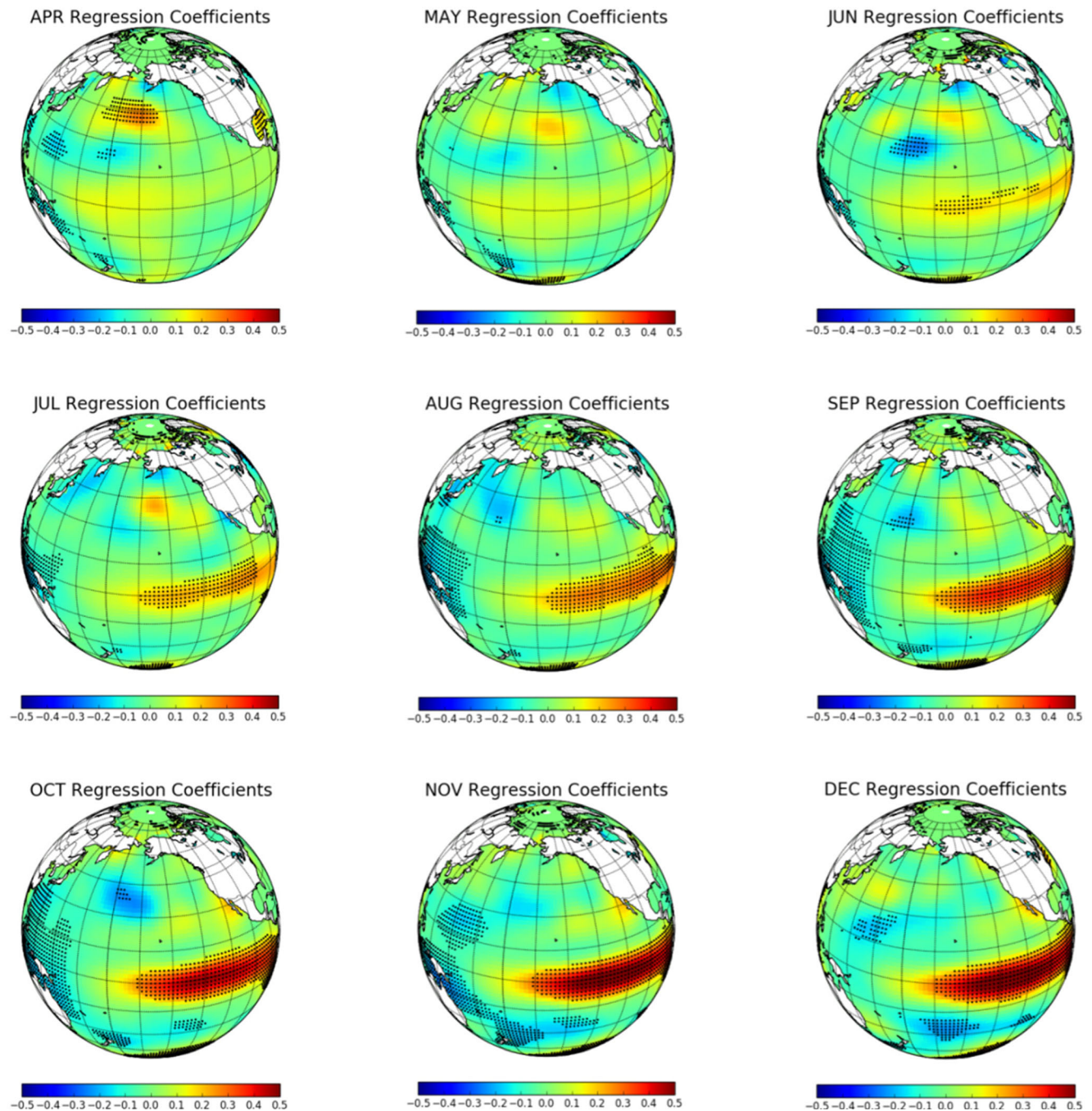
Fig. 6 Maps of SSTs of April to December regressed on to December mean EOT-1
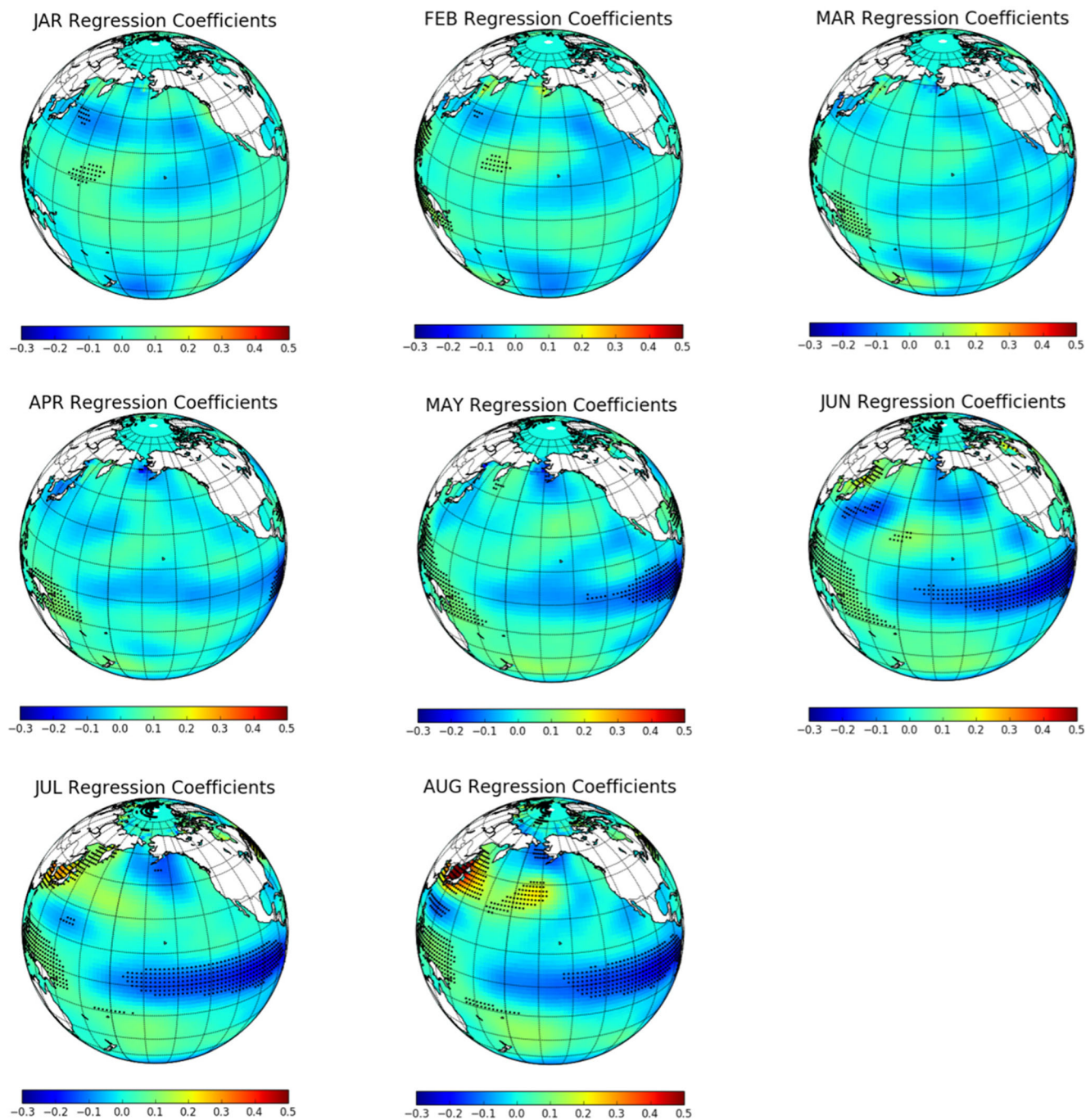
Fig. 7 Maps of SSTs of January to August regressed on to August mean EOT-1

the Pacific Ocean SSTs onto August and December EOT-1 modes for mean temperature demonstrate that the leading EOTs show notable lagged and concurrent regression with strong ENSO signals over the equatorial Pacific. The December lag regression suggests noticeable predictability from tropical Pacific Ocean SST with positive regression coefficients decreasing as the lag increases. The lagged regression signals were detected from July to December, and then

the Pacific SST-related temperature signals strongly diminish. The August lag-0 to lag-4 regression representing regression April to August SSTs onto August EOT-1 indicates a negative correlation with tropical Pacific cold tongue SSTs. The negative signals extend to months prior to May at lag-3 and then do not exhibit substantial amplitude during January to April. Lag regression maps indicate coherent Pacific Ocean SST variability related to EOTs of Korean temperature. Despite noise in

the SST-temperature relationship, the sources identified above may provide promise to improve prediction of South Korea monthly mean temperature variations.

In October and December for extreme high and low temperature, there is a different tendency in the ENSO-temperature relationship. The lagged and concurrent SST regression onto
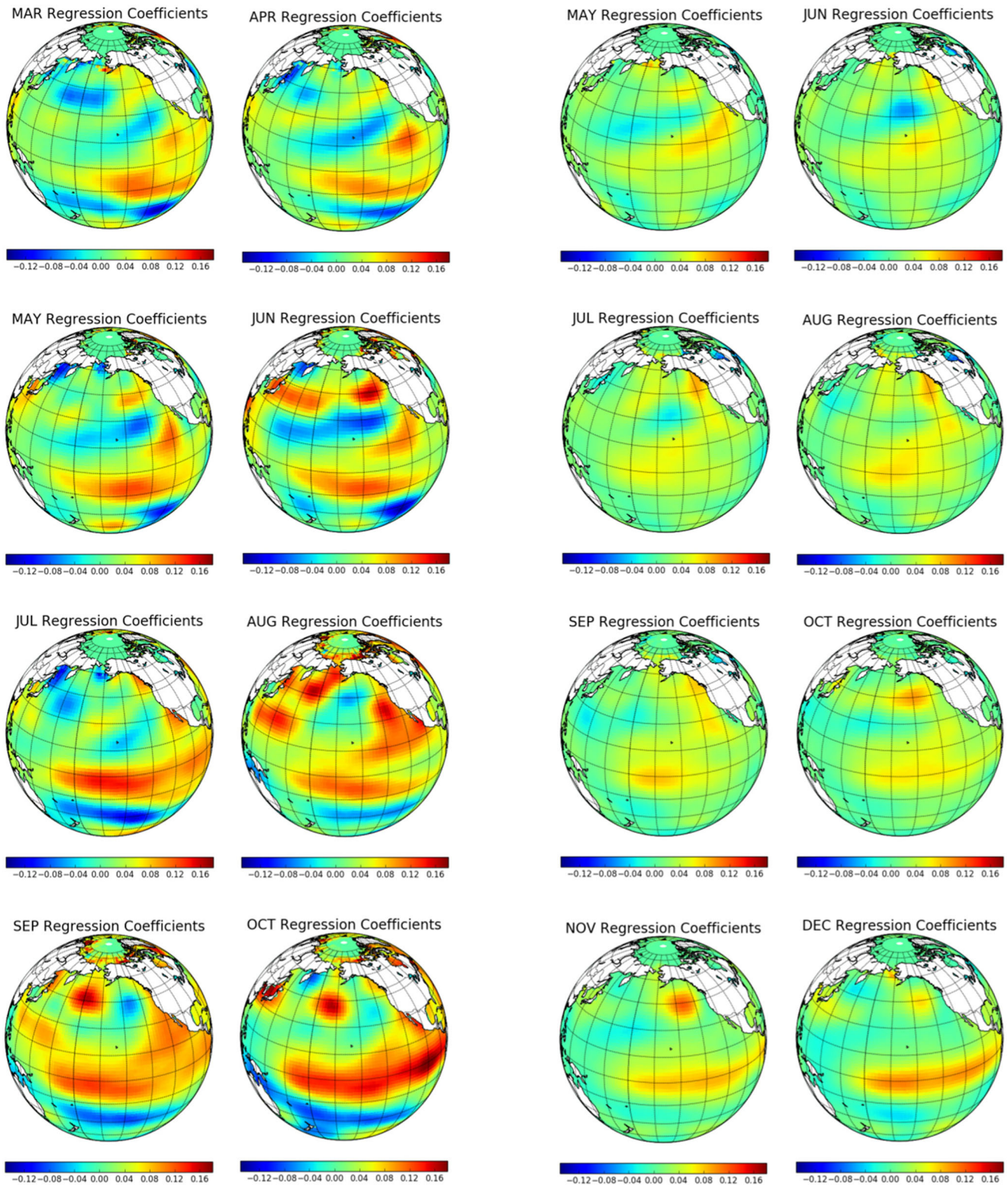

Fig. 8 Maps of lag-0 to lag-7 SSTs regressed on to October EOT-1 of extreme high temperature (left eight panels) and December EOT-1 of extreme low temperature (right eight panels)

the leading EOT-1 for extreme high-temperature anomaly in October and extreme low-temperature anomaly in December account for the aforementioned different tendency as shown in Fig. 8. These lag regression maps show that the regression coefficients of very warm extremes in October from Pacific SSTs are more evident than that of very cold December extremes. The lower predictability of January–April leading EOTs is attributed to weaker SST-temperature relationships in this time of year. Consequently, these findings of the potential sources of climate predictability indicate important implications for the seasonal forecasting the major thermodynamic extremes of unusually severe cold weather and abnormal heat wave.

7 Discussion

The main focus of this analysis is to expand upon findings from the previous studies such as Halpert and Ropelewski (1992) and Lee and Julien (2015) that documented teleconnections between the tropical ENSO forcing and the midlatitude temperature variability. In the global-scale study that employed harmonic analysis, Halpert and Ropelewski (1992) noted consistent relationships between East Asian temperature patterns and both warm and cold phases of ENSO. In more regionally focused analysis, Halpert and Ropelewski (1992) also documented that northwest North America and Japan exhibit negative temperature anomalies during ENSO cold events during northern Hemisphere winter. These results are consistent with the outcomes of the current study that shows similar responses in Korean temperature associated with tropical ENSO forcing. However, visual inspection of the station location maps in previous papers indicates that the significant ENSO-temperature relationships over South Korea we identify were not sufficiently resolved due to the data coverage limitations. Our study resolves these issues through use of a high-quality, high-resolution Korean surface dataset and also provides additional information on the CI-temperature linkage over East Asia which was not identified in previous studies.

The EOT decomposition and cross-correlation analysis described in the previous section demonstrate that the leading mode of August South Korean temperature has a negative correlation with SST over the equatorial Pacific Ocean, while that of December temperature shows a positive correlation with tropical Pacific SST variability. In other words, during warm ENSO years below-normal Korean temperature anomalies are observed in August, while above-normal temperature departures are observed in December. For ENSO cold phase years, the opposite is true. Figure 9 illustrates a comparison of standardized temperature anomalies for mean temperatures in August and December during the warm and cold event years using the monthly temperature data for the entire stations over South Korea. The scatterplots for the warm ENSO phase are

mostly distributed in the upper left part of the plot, while those for the cold phase are distributed in lower right part. These notable patterns for monthly mean temperature data suggest that August and December are characterized by opposite signed tendency for an ENSO event of a given sign.

The correlation pattern between the Korean temperature EOT and the Pacific Ocean (PO)-Indian Ocean (IO) SST shows noticeable differences from summer to winter. In fall and winter, the Korean temperature variability shows a significant positive correlation with the PO-IO SST, while negative correlation is true in August. These opposite correlation patterns are very similar to the positive and negative phases of ENSO and IOD episodes, implying that both extreme events have a close relationship with the Korean temperature variability. Why does the IO-PO SST pattern positively correlate with the Korean temperature in fall-winter but negatively correlate with the Korean temperature in August? The tropical PO-IO sea surface temperature can cause large anomalous circulation over the WNP (Wu et al. 2000). Hence, one way by which the SST variation over the tropical PO-IO has an effect on the Korean temperature is through the atmospheric circulation over the WNP. For these seasons, the different responses of atmospheric circulation over East Asia to distinct tropical PO-IO SST variation may play a critical role in the different correlation patterns. Thus, we focus on the influences of different PO-IO SST patterns on the atmospheric circulation anomalies over East Asia.
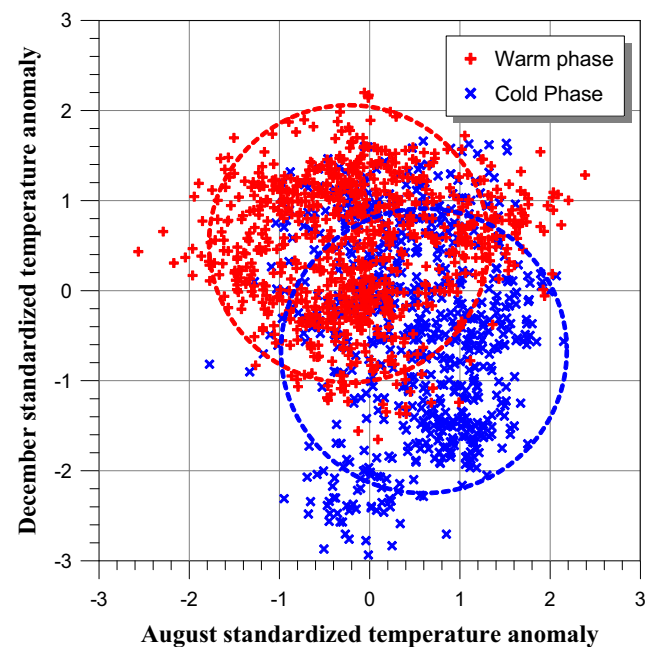

Fig. 9 The comparison of standardized temperature anomalies for below (above) normal temperature in August and above (below) normal temperature in December during the warm (cold) phase of ENSO events using the monthly temperature time series. The dashed circles indicate the location and pattern of the distribution densities of the symbols based on each center of the warm and cold phases

To examine what causes the anomalous temperature over the Korean peninsula, circulation anomalies associated with ENSO forcing is investigated using composite difference of circulation fields, e.g., the 500-hPa geopotential height and 850-hPa vector winds, between high and low ENSO years as shown in Fig. 10. Following the criteria suggested by Lee and Julien (2016), the years 1982, 1987, 1991, 1997, 2009, and 2015 are identified as extreme positive events, while 1973, 1975, 1988, 1999, 2007, and 2011 are designated as extreme negative events. In August, there is a cyclonic circulation over the subtropical North Pacific as shown in Fig. 10a. The cyclonic flow can be interpreted as Rossby wave response to the equatorial Pacific heating. The northerlies prevailing over the Korean peninsula (Fig. 10b) is part of the anomalous cyclonic circulation over the subtropical North Pacific. This figure clearly describes the Korean peninsula under the influence of dominant northerly wind. Son et al. (2014) suggested that the anomalous cyclonic circulation over the subtropical North Pacific is a principal driver in teleconnection between ENSO forcing and the Korean climatic variation. The corresponding northerly wind cut-off the warm air supply from

equator towards the Korean peninsula resulting in below-normal temperature activity.

On the other hand, in December (Fig. 10c), a massive anomalous anticyclone is found over the WNP with two centers, one located in the midlatitude region over the Kuroshio extension and another located over the Philippine Sea. Wang et al. (2000) suggested that the WNP anticyclone is an important driver that links the East Asian winter monsoon and the central-eastern Pacific warming. As shown in Figures 11b, anomalous southwesterly wind prevails over the Korean peninsula and the northwestern part of the Philippine Sea anticyclone, reflecting damping phases of East Asia winter monsoon or a warmer than normal in winter. The anomalous southerly wind transports warm air toward the Korean peninsula. This northward transport is attributed to a warmer than normal temperature over the Korean peninsula.

To investigate the atmospheric circulation patterns associated with the tropical Indian Ocean SST, composite differences of the 500-hPa geopotential height and 850-hPa vector winds between high and low IOD years are computed as shown in Fig. 12. Following the criteria suggested by Saji et al. (1999),

Fig. 10 Composite differences of 500-hPa geopotential height (left) and 850-hPa vector wind (right) between the high and low ENSO years in August

(a)

(b)
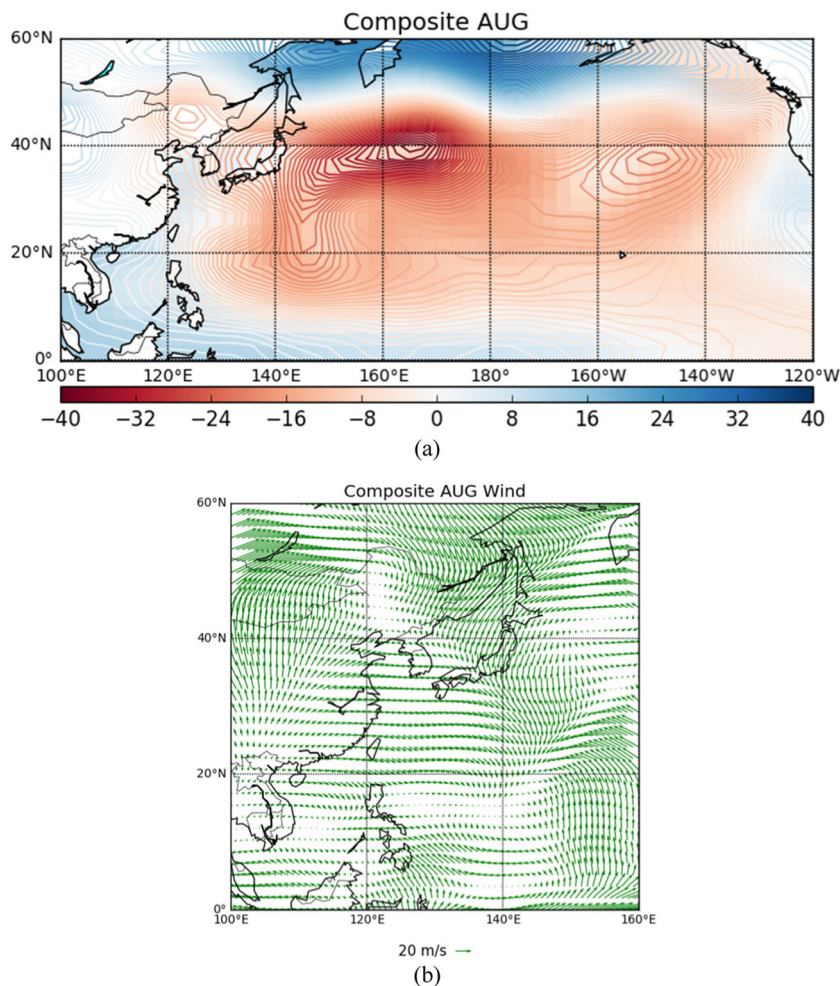
the years 1982, 1983, 1994, 1997, 2006, and 2012 are identified as extreme positive events, while 1975, 1989, 1992, 1996, 1998, and 2010 are designated as extreme negative events. The North Pacific Subtropical High (NPSH) shifts slightly north-westward from its normal position in October and November (Fig. 11a, c). This shift of the NPSH induces the intensification of the southerly winds at the western edge of the NPSH. This results in the strengthening of the cross-equatorial flow over the WNP region, which causes more warm air supply from the tropical Pacific Ocean to the Korean peninsula. Hence, the Korean peninsula could be under the influence of anomalous southerlies transporting the warm air from equator. The composite differences of 850-hPa vector wind between the high and low IOD episodes are shown in Fig. 11b, d. Consistent with the composite difference pattern for the geopotential field, anticyclonic flow exists in the areas of positive geopotential anomalies, while cyclonic flow is located in the areas of negative geopotential anomalies. The figure clearly describes the Korean peninsula under the influence of distinct anomalous southerly wind. The southerly winds are anomalously strong and bring warm air from the lower latitudes to the Korean peninsula. Thus, the strong anomalous southerlies modulate

the warm air supply towards the Korean peninsula causing above-normal temperature (Fig. 12).

The contrast of the relationship between the extreme ENSO-IOD phases and the anomalous circulation over the WNP indicates the strengthened inter-link between the anomalous circulation over East Asian and the extreme phases of the tropical PO-IO in summer to winter. The change in the climatic linkage between the surface sea temperature over tropical PO-IO and the anomalous circulation over the WNP shows that the influence of the tropical PO-IO SST variation on the Korean temperature through the anomalous WNP circulation is different in August and October–December. These patterns of PO-IO SST tend to modulate the intensification or suppression of the WNP circulation anomalies and would lead to a strong positive or negative temperature anomaly.

The overall results of the current analyses are in general agreement with those of other recent studies regarding the impacts of ENSO on thermodynamic variables over the Korean peninsula. Cha et al. (1999) examined the teleconnection between remote ENSO forcing and Korean variables such as temperature, atmospheric circulation, and precipitation, and revealed that tropical

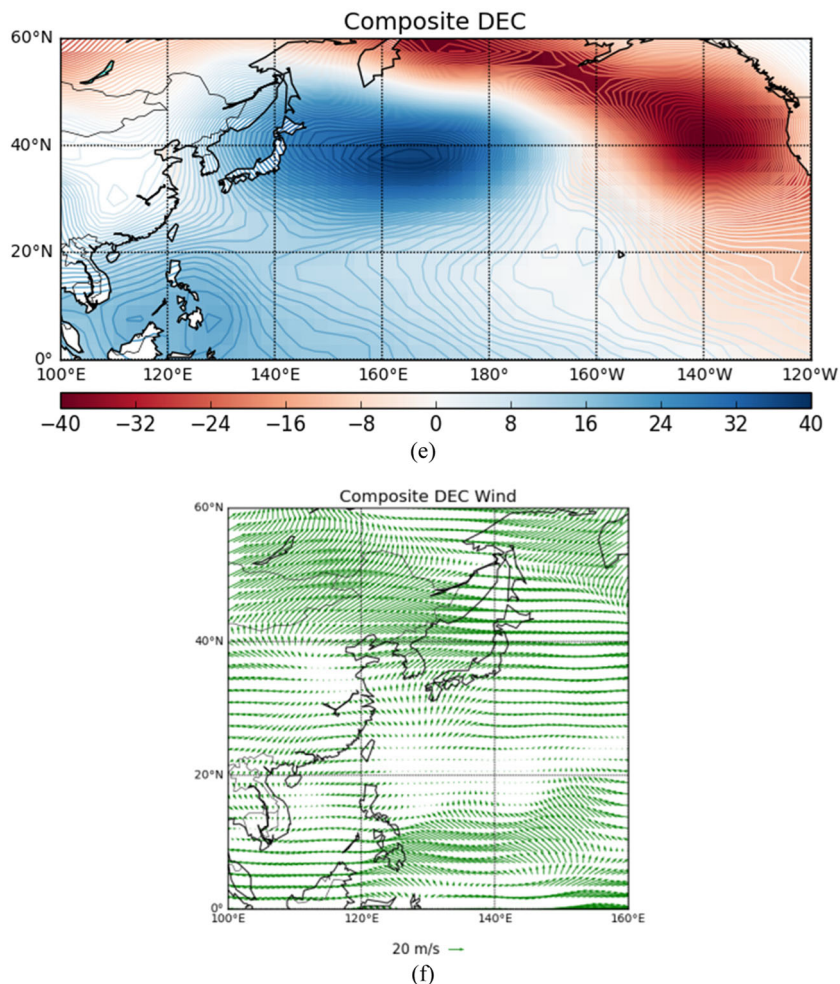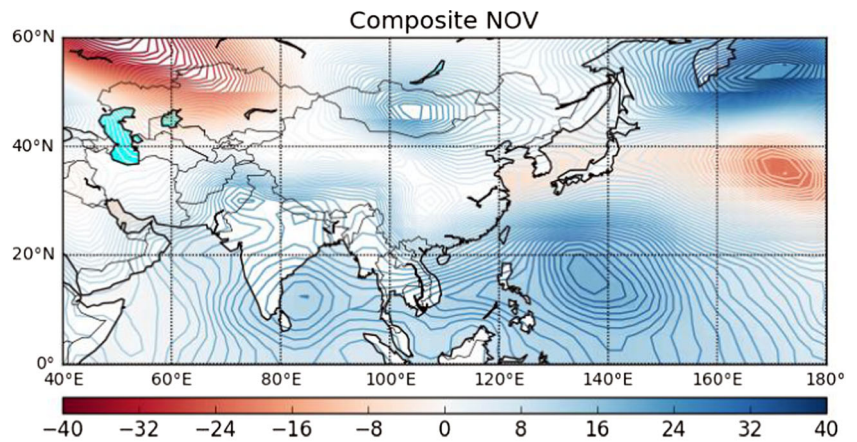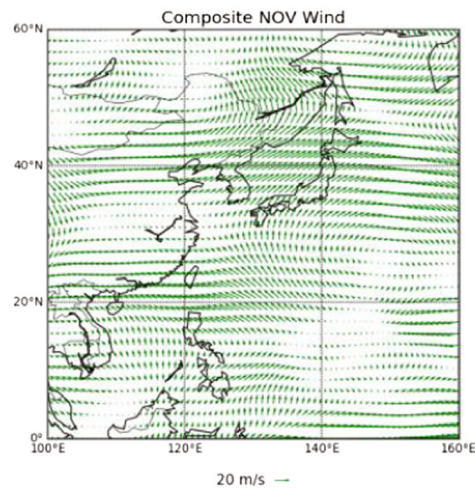**Fig. 11** As in Fig. 10, but for IOD years in December

(e)

(f)

(c)

(d)

Fig. 12 As in Fig. 10, but for IOD years in November

ENSO forcing has an important impact on fluctuations of seasonal temperature over South Korea resulting in negative temperature anomalies in summer and positive temperature anomalies in winter during ENSO warm events. In addition, our analysis is also consistent with the findings by Kang (1998) and Min and Yang (1998) who demonstrated the tendency for negative and positive Korean temperature responses to warm ENSO SSTs in summer and winter, respectively. Although they nicely demonstrated the statistical process of ENSO impacts on South Korea, the study has a limitation in explaining the impact on monthly basis. Their studies are based on the seasonal mean data for only about a dozen stations by assuming that the relation is nearly uniform within one season. Even though the tropical sea surface temperature (SST) forcing associated ENSO is quite steady within a season, there is a strong seasonality in regional climate variables. The present study demonstrated the far-reaching effects of climate indicators on monthly mean and extreme temperature variability based on a high-quality, high-resolution Korean surface dataset.

8 Summary and conclusions

In the current study, we apply an empirical orthogonal teleconnection (EOT) decomposition technique to mean and extreme South Korean temperatures to quantify the remote impacts of large-scale modes of climate variability as quantified through climate indices (CIs). We demonstrated the potential for prediction of these temperature patterns based on knowledge of monthly tropical SST fields using cross-correlation and lag regression analysis for the leading EOT modes and ENSO and IOD indicators.

The spatiotemporal features of mean (extreme high) temperatures over South Korea are dominated by an eastern (southern) coastal mode during summer and northern (middle) inland mode in winter, while extreme low temperature exhibits a northern inland mode in summer and western coastal mode in winter. The temporal evolution of the leading EOT modes exhibits a mostly increasing trend and an interdecadal oscillation. The leading mean temperature EOT modes explain more of the variance in Korean temperature variability than the leading extreme EOT modes. The MEI

time series that explain tropical Pacific ENSO variability have significant negative correlations with the leading EOTs of mean temperature in August and September, whereas the leading EOTs for December exhibit positive correlations with the MEI time series. The leading EOT mode of mean Korean temperature is significantly positively correlated with the boreal fall IOD as quantified by the DMI index, while the extreme EOT-1 mode shows a positive correlation with Indian Ocean SST anomalies in boreal fall. The leading EOTs for mean and extreme temperatures also exhibit a significant negative correlation with an index of monsoon variability over the WNP region in December. The leading EOTs for October temperature exhibit the positive correlation with the tropical cyclone variability, while the leading EOTs for mean and extreme high temperature exhibit significant negative correlations with the EESI in November. From the results of cross-correlation and lag regression analyses, the leading EOTs for August and December mean Korean temperatures have predictability up to 5 months of lead time from tropical Pacific SSTs, while potentially predictable responses of fall season temperature from Indian Ocean SSTs were detected up to 4 months in advance. Also, the regression coefficients of the tropical Pacific SSTs onto very warm extremes in October are more evident than that for very cold December extremes.

The methodological approaches described here do not take into consideration the type of ENSO event, which is often categorized into classical El Niño and El Niño Modoki based on the location of peak SST anomalies. Further investigation of the teleconnected responses for the two types of ENSO events on thermodynamic variables in the extratropics including Korea needs to be performed in more detail.

References

Ahn JB, Ryu JH, Cho EH, Park JY (1997) A study of correlations between air-temperature and precipitation in Korean and SST over the tropical Pacific. J Korean Meteor Soc. 33(3):487–495

Bradley RS, Diaz HF, Kiladis GN, Eischeid JK (1987) ENSO signal in continental temperature and precipitation records. Nature 327:487–501

Cha EJ (2007) El Niño-Southern Oscillation, Indian Ocean Dipole mode, a relationship between the two phenomena, and their impact on the climate over the Korean Peninsula. J Korean Earth Sci Soc 28(1):35–44

Cha EJ, Jhun JG, Chung HS (1999) A study on characteristics of climate in South Korea for El Niño/La Niña years. J KMS 35(1):99–117

Daly C, Neilson PR, Phillips DL (1994) A statistical-topographic model for mapping climatological precipitation over mountainous terrain. J Appl Meteorol 33:140–158

Ha, K.J., 1995. Interannual variabilities of wintertime Seoul temperature and the correlation with Pacific Sea surface temperature. J Korean Meteorol Soc 31: 313–323 (in Korean)

Halpert MS, Ropelewski CF (1992) Surface temperature patterns associated with the Southern Oscillation. J Clim 5:557–593

Huang B, Banzon VF, Freeman E, Lawrimore J, Liu W, Peterson TC, Smith TM, Thorne PW, Woodruff SD, Zhang HM (2014) Extended Reconstructed Sea Surface Temperature version 4 (ERSST.v4): part I. Upgrades and intercomparisons. J Clim. https://doi.org/10.1175/JCLI-D-14-00006.1

Jung HS, Choi YE, Oh JH, Lim GH (2002) Recent Trends In Temperature And Precipitation Over South Korea. Int J Climatol 22:1327–1337

Kang IS (1998) Relationship between El-Niño and Korean climate variability. J Korean Meteor Soc 34(3):390–396

Karabörk MÇ, Kahya E (2007) The links between the categorized Southern Oscillation indicators and precipitation patterns over Turkey. Hydrol Days 2007 87–89

Kiladis GN, Diaz HF (1989) Global climatic anomalies associated with extremes in the Southern Oscillation. J Clim 2:1069–1090

Kiladis GN, van Loon H (1988) The Southern Oscillation. Part VII: meteorological anomalies over the Indian and Pacific sectors associated with the extremes of the oscillation. Mon Weather Rev 116:120–136

Kim MK, Kang IS, Park CK, Kim KM (2004) Super ensemble prediction of regional precipitation over Korea. Int J Climatol 24:777–790

King AD, Klingaman NP, Alexander LV, Donat MG, Jourdain NC, Maher P (2014) Extreme rainfall variability in Australia: patterns, drivers, and predictability. J Clim 27:6035–6050

Klingaman NP, Woolnough SJ, Syktus J (2013) On the drivers of inter-annual and decadal rainfall variability in Queensland, Australia. Int J Climatol 33:2413–2430

Knapp KR, Kruk MC, Levinson DH, Diamond HJ, Neumann CJ (2010) The international best track archive for climate stewardship (ibtracs): Unifying tropical cyclone best track data. Bull Am Meteorol Soc 91:363–376

Korea Meteorological Administration (KMA) (2018) Annual Climatological Report. 13:11–12 (in Korean)

Kripalani RH, Oh JH, Chaudhari HS (2010) Delayed influence of the Indian Ocean Dipole mode on the East Asia–West Pacific monsoon: possible mechanism. Int J Climatol 30:197–209

Lee DR (1998) Relationships of El Niño and La Niña with both temperature and precipitation in South Korea. J Korea Water Resour Assoc 31(6):807–819 (in Korean)

Lee JH, Julien PY (2015) ENSO impacts on temperature over South Korea. Int J Climatol 10:1002/4581

Lee JH, Julien PY (2016) Teleconnections of the ENSO and South Korean precipitation patterns. J Hydrol 534:237–250

Lee JH, Julien PY (2017) Influence of the El Niño/Southern Oscillation on South Korean streamflow variability. Hydrol Process 10. https://doi.org/10.1002/hyp.11168

McKee, T.B., Doesken, N.J., Kleist, J., 1993. The relationship of drought frequency and duration to time series. 8th Conference on Applied Climatology, Anaheim, CA 1993 pp. 179–187

Min, W. K, Yang, J.S., 1998. A study on correlation between El-Nino and winter temperature and precipitation in Korea. J Korean Assoc Reg Geograph 4 (2): 151–164 (in Korean)

Redmond KT, Koch RW (1991) Surface climate and streamflow variability in the western United States and their relationship to large circulation indices. Water Resour Res 27(9):2381–2399

Ropelewski CF, Halpert MS (1986) North American precipitation and temperature patterns associated with El-Niño Southern Oscillation (ENSO). Mon Weather Rev 114:2165–2352

Saji NH, Yamagata T (2003) Possible impacts of Indian Ocean Dipole Mode events on global climate. Clim Res 25:151–169

Saji NH, Goswami BN, Vinayachandran PN, Yamagata T (1999) A dipole mode in the tropical Indian Ocean. Nature 401:360–363

Son HY, Park JY, Kug JS, Yoo J, Kim CH (2014) Winter precipitation variability over Korean Peninsula associated with ENSO. Clim Dyn 42:3171–3186

Stephan CC, Klingaman NP, Vidale PL, Turner AG, Demory M-E, Guo L (2018a) A comprehensive analysis of coherent rainfall patterns in China and potential drivers. Part I: interannual variability. Clim Dyn 50:4405–4424

Stephan CC, Klingaman NP, Vidale PL, Turner AG, Demory M-E, Guo L (2018b) A comprehensive analysis of coherent rainfall patterns in China and potential drivers. Part II: Intraseasonal variability. Clim Dyn 51:17–33

Van den Dool HM, Saha S, Johansson Å (2000) Empirical orthogonal teleconnections. J Clim 13:1421–1435

van Loon H, Madden R (1981) The Southern Oscillation. Part I: global associations with pressure and temperature in northern winter. Mon Weather Rev 109:1150–1162

Walker GT (1923) Correlation in seasonal variations of weather, VIII: a preliminary study of world weather. Mem Indian Meteorol Dep 24: 75–131

Wang B, Wu R, Fu X (2000) Pacific–East Asian teleconnection: How does ENSO affect east Asian climate. J Clim 13:1517–1536

Wang B, Xiang B, Lee J (2013) Subtropical high predictability establishes a promising way for monsoon and tropical storm predictions. Proc Natl Acad Sci U S A 110:2718–2722

Wu R, Wang B (2002) A Contrast of the East Asian Summer Monsoon–ENSO Relationship between 1962–77 and 1978–93. J Clim 15: 3266–3279